Ocean Modelling 136 (2019) 107–119

Contents lists available at ScienceDirect

Ocean Modelling

journal homepage: www.elsevier.com/locate/ocemod

Numerical analysis of boundary conditions in a Lagrangian particle model for vertical mixing, transport and surfacing of buoyant particles in the water column

Tor Nordam[a,b,*], Ruben Kristiansen[b], Raymond Nepstad[a], Johannes Röhrs[c]

[a] SINTEF Ocean, Trondheim, Norway
[b] Norwegian University of Science and Technology, Trondheim, Norway
[c] Norwegian Meteorological Institute, Oslo, Norway

ARTICLE INFO

Keywords:
Oil spills
Fish eggs
Microplastics
Vertical mixing
Random walk

ABSTRACT

Lagrangian particle models are used for many applications in the ocean sciences, including transport modelling of oil spills, fish eggs and larvae, plastics, and sediment particles. In the context of oil spill modelling, there are numerous papers discussing entrainment of surface oil by breaking waves. However, for the opposite process, *i.e.*, droplets reaching the surface and joining the surface slick, we have found no discussion in the literature of the exact steps involved. Given the wide use of particle-based models in oil spill modelling, it is important to establish a consistent recipe for treating the surface boundary.

We investigate a Lagrangian particle model for the vertical transport, surfacing and resuspension of buoyant material in the water column. By modifying the behaviour at the surface boundary, the model can be applied to materials such as oil droplets, that form a surface slick, and hence see the surface as an absorbing boundary, and to particles that do not form a surface slick, such as fish eggs and microplastics. For slick-forming materials, we also consider resuspension from the surface slick, (*e.g.*, entrainment of surface oil by breaking waves). While we restrict our attention to positively buoyant materials, the model is equally applicable to the settling of negatively buoyant particles, such as sediment grains and marine snow.

We consider three case studies, each designed to allow a detailed and direct comparison of the Lagrangian model to an Eulerian model based on numerical solution of the advection-diffusion-reaction equation. We demonstrate that the two models give the same results when the boundary at the surface is treated correctly.

1. Introduction

Lagrangian transport models are commonly used in many areas of ocean-related science, including the modelling of oil spills (Dagestad et al., 2018; De Dominicis et al., 2013; French-McCay, 2009; García-Martínez and Flores-Tovar, 1999; Mariano et al., 2011; Reed et al., 2000), microplastics (Ballent et al., 2013), ichtyoplankton (Castano-Primo et al., 2014; Fox et al., 2009; Thygesen and Ådlandsvik, 2007), fish eggs (Röhrs et al., 2014), and mineral particles (Gräwe and Wolff, 2010). The relative simplicity of the core Lagrangian particle scheme makes it attractive for numerical applications, however, there are several subtle points which must be carefully addressed in oceanic applications (Brickman and Smith, 2002; Ross and Sharples, 2004; van Sebille et al., 2018). For example, common to all of these applications is that the models must correctly treat the boundaries at the sea surface and the seabed. Furthermore, in the case of spatially variable diffusion, which is usually the case in the ocean, care must be taken to avoid numerical artefacts that result from a naïve formulation of random walk (Hunter et al., 1993; Visser, 1997).

In the field of numerical oil spill modelling, it has long been recognised that the vertical distribution of oil is of paramount importance. This includes both the vertical distribution of submerged oil, and the distinction between surface oil and submerged droplets. One of the earliest works treating an oil spill as a three-dimensional process is that of Elliott (1986). Elliott described the elongation of an oil slick in the direction of the wind, attributing the effect to vertical current shear, and also formulated a three-dimensional random-walk based particle model. While that model allowed sufficiently large oil droplets to remain at the surface, as their rise due to buoyancy would always dominate over the random displacement due to diffusion, it did not include a slick formation process or a separate surface state.

Since Elliott (1986), much has been written about natural

* Corresponding author.
E-mail address: tor.nordam@sintef.no (T. Nordam).

https://doi.org/10.1016/j.ocemod.2019.03.003
Received 24 January 2019; Received in revised form 25 February 2019; Accepted 3 March 2019
Available online 05 March 2019

entrainment, *i.e.*, the process where surface oil is submerged as droplets due to dissipation of surface gravity waves. Several different models have been developed for both the rate of entrainment and the resulting droplet size distribution (see, *e.g.*, Delvigne and Sweeney (1988), Johansen et al. (2015), Li et al. (2017)). However, less has been said about the opposite process, *i.e.*, oil droplets reaching the surface due to buoyancy and merging with a surface slick. Reviews of the field, such as Spaulding (1988), ASCE (1996), Reed et al. (1999), and Spaulding (2017) all discuss entrainment of surface oil and vertical transport and mixing of droplets, but contain no details of the surfacing process. In the context of Eulerian models, surfacing is discussed by, *e.g.*, Tkalich and Chan (2002), but to the best of our knowledge, a complete description of the steps involved in calculating surfacing in a particle-based oil spill model has not been published.

In the current paper, we provide a direct comparison between the Lagrangian particle scheme, and an Eulerian model based on the advection-diffusion-reaction (ADR) equation, focusing particularly on the treatment of the surface. To this end, we provide a detailed description of a Lagrangian particle model for the vertical mixing, transport and surfacing of oil droplets in the water column, as well as the vertical mixing and transport of non-slick-forming particles such as fish eggs and microplastics. For the case of oil droplets, we also include resuspension from the surface slick into the water column, which can for example be caused by breaking waves. We then formulate an equivalent Eulerian model, based on the ADR equation, with appropriate boundary conditions. While we consider positively buoyant material throughout this paper, the formulated models and the results are equally applicable to settling, and optionally resuspension, of negatively buoyant particles.

We consider three case studies, which are designed to allow a direct comparison of the Lagrangian and Eulerian schemes. For each case, we provide details of all the steps involved in the Lagrangian particle model, and a complete description of an equivalent Eulerian scheme with specific boundary conditions. We then demonstrate that we obtain the same results with the two models.

The layout of the paper is as follows: In the following section (Section 2) we describe the system to be studied, *i.e.*, buoyant material in the water column, and how this material may or may not form a continuous slick at the surface, and how a continuous slick may be resuspended as droplets due to breaking waves. We then formulate two models for this system, a Lagrangian model based on particles subjected to buoyant rise, random walk and resuspension, and an Eulerian model based on the ADR equation. In Section 3 we consider three different case studies, and present the results of simulating all three cases with both models. Section 4 contains a discussion of the way we have chosen to treat the boundary, both for the Lagrangian and Eulerian schemes. Finally, in Section 5, we provide some concluding remarks. The Appendices expand on some of the technical details of solving the ADR equation numerically, and on the choice of numerical parameters for the particle model.

2. Models for buoyant material in the water column

We consider a system where some buoyant material (*e.g.*, microplastics, fish eggs or oil droplets) is dispersed in the water column. We will only consider transport in the vertical direction, treating the water column as a one-dimensional system, and we consider positively buoyant particles rising at their terminal velocity.

The main source of vertical mixing in the ocean is turbulent diffusion, which is orders of magnitude greater than molecular diffusion (Tennekes and Lumley, 1972). Vertical turbulent diffusion is usually described by an eddy diffusivity profile, here denoted as $K(z)$, which gives the diffusivity as a function of depth. Eddy diffusivity profiles can, for example, be obtained from ocean models (*e.g.*, ROMS[1]), from specialised turbulence models (*e.g.*, GOTM[2]) or from simpler analytical expressions seeking to capture some important features for a given scenario (see, *e.g.*, Large et al. (1994)).

Depending on the type of material, the surface may or may not be seen as a partially absorbing boundary. Materials that do not form surface slicks, such as fish eggs and microplastics, may reach the surface through buoyancy, and later be resuspended due to turbulent eddies in the water. Hence, we may formulate the following rules, which when repeatedly applied describe the motion of non-slick-forming buoyant particles in a turbulent water column:

- Particles are randomly displaced, due to turbulent motion of the water. Being caused by the motion of the water, this random displacement treats the surface as a reflecting boundary.
- Particles rise due to buoyancy. When particles reach the surface due to buoyancy, they can rise no further, thus treating the surface as a barrier.

The rationale for treating the boundary as reflecting in diffusion is that turbulent diffusion is caused by eddies in the water, and, being formed by water, these eddies are necessarily unable to carry material *out* of the water.

In the case of oil droplets, a continuous slick may be formed at the surface, and as a droplet rises to the surface and merges with the slick, it is effectively removed from the water column. For an oil slick to be broken up into droplets and resuspended, a high-energy event such as a breaking wave is required. A set of rules describing the motion of slick-forming, buoyant particles is:

- Droplets are randomly displaced, due to turbulent motion of the water. Being caused by the motion of the water, this random displacement treats the surface as a reflecting boundary.
- Droplets rise due to buoyancy. When droplets reach the surface due to buoyancy, they become part of the surface slick, thus treating the surface as an absorbing boundary.
- Once part of the surface slick, droplets may be resuspended due to breaking waves, at some rate which is related to the wave state. Droplets resuspended due to waves are distributed into the upper part of the water column, and may in general be assigned a new size in the process.

Again, the rationale for the reflecting boundary in the diffusion step is that material carried by the motion of the water cannot leave the water. Furthermore, if the surface was absorbing in diffusion, increasing the diffusivity could lead to arbitrarily fast surfacing, which is contrary to what is observed in reality.

In what follows, we will formulate an Eulerian and a Lagrangian model for the behaviour described above. Common to both models is that they operate in discrete time, and that we consider a fixed timestep, Δt, where

$$t_n = t_0 + n\Delta t, \tag{1}$$

and where t_0 is the time at the start of the simulation.

2.1. Lagrangian model

In a Lagrangian particle model, an ensemble of a large number, N_p, of particles is used to describe the effects of advection and diffusion. At each timestep, each particle undergoes a random displacement due to diffusion, and a directed displacement due to buoyancy. The step length in the random displacement is found from the diffusivity profile, $K(z)$.

For the random walk formulation to be consistent, it must obey the rule that an initially well-mixed passive (*i.e.*, neutrally buoyant) tracer

[1] myroms.org

[2] gotm.net

must remain well mixed, regardless of the diffusivity profile. This is known as the well-mixed condition, and was first formulated by Thomson (1987). As has been pointed out by several authors (see, *e.g.*, Holloway (1994), Hunter et al. (1993), van Sebille et al. (2018), Visser (1997)), a naïve formulation of the random walk will cause an unphysical net transport away from areas of high diffusivity, and thus will not obey the well-mixed condition. Additionally, care must be taken near the boundaries of the computational domain, as the shape and properties of the diffusivity function here can impact the accuracy of the results (Ross and Sharples, 2004). We will return to this last point in greater detail in Sections 3 and 4.

We implement a random walk algorithm known as the Visser scheme (Gräwe, 2011; Visser, 1997), where a particle which at time t_n is at a depth z_n, at a time $t_{n+1} = t_n + \Delta t$ will be at a new position $z_{n+1} = z_n + \xi(z_n)$, where the displacement $\xi(z_n)$ is given by

$$\xi(z_n) = K'(z_n)\Delta t + R\sqrt{\frac{2}{r}\Delta t K\left(z_n + K'(z_n)\frac{\Delta t}{2}\right)}, \tag{2}$$

where $K'(z_n) = \frac{\mathrm{d}K}{\mathrm{d}z}\Big|_{z_n}$, Δt is the timestep of the model, and R is a random process with mean $\langle R\rangle = 0$, and variance $\langle R^2\rangle = r$. Throughout this paper, we have taken R to be uniformly distributed random numbers between -1 and 1, in which case $r = 1/3$.

The Visser scheme will obey the aforementioned well-mixed condition, provided the timestep is sufficiently short. The requirement is essentially that the diffusivity profile is well approximated by a linear function over the step length of the random walk (Visser, 1997). This is satisfied if

$$\Delta t \ll \min\left(\frac{1}{|K''(z)|}\right), \tag{3}$$

where $K''(z) = \frac{\mathrm{d}^2K}{\mathrm{d}z^2}$, and the minimum is taken over the entire water column. According to Gräwe et al. (2012), it is generally agreed that the timestep should be kept at least an order of magnitude below the limit given by Eq. (3).

The rise due to buoyancy is simply implemented as a constant, upwards displacement equal to $-v_b\Delta t$ at each timestep (we take depth to be positive downwards). This is because particles are considered to rise at their terminal velocity. For small particles with small rise velocities, this is a good approximation, as the terminal velocity is reached very fast compared to other relevant processes.

As previously discussed, what happens when a particle reaches the surface depends on the particular type of material considered. In the context of an oil spill simulation, a droplet that surfaces is assumed to be absorbed into a continuous surface slick of oil, and will not be mixed back down into the water column by the eddy diffusivity alone. Hence, an oil droplet that has surfaced is (temporarily) removed from the water column. For a non-slick-forming particle such as a piece of microplastic, the situation may be different, and the eddy diffusivity may be sufficient to move the particle back down into the water column.

Particles that have surfaced and been absorbed into a surface slick may however be resuspended due to breaking waves, as would be the case for oil droplets. We have chosen to include this in the model for slick-forming materials[3] by optionally submerging a constant fraction of the surface slick at each timestep. This corresponds to an exponential decay of the amount of material at the surface, with a decay rate λ, which is related to the wave state, typically calculated via the whitecap fraction (Li et al., 2017; Scanlon et al., 2016). The entrainment is included in the particle model by giving each surfaced particle a probability of being mixed down at each timestep, calculated from the lifetime, $\tau = 1/\lambda$, at the surface. When a particle is resuspended, it is placed at a random depth, uniformly distributed between the surface ($z = 0$) and a depth $z = L$ (Tkalich and Chan, 2002). In practice, the entrainment depth is related to the wave height (Delvigne and Sweeney, 1988) or the intrusion depth of breaking waves (Leifer and De Leeuw, 2006). In a more realistic model, a resuspended particle would also be assigned a new size, randomly drawn from a suitable size distribution (see, *e.g.*, Delvigne and Sweeney (1988), Johansen et al. (2015), Li et al. (2017)). However, these complications are outside the scope of the current study, which is focused on the process of surfacing.

This model can be formulated as a series of operations carried out for each particle, during each timestep, in order to calculate the position, z_{n+1}, at time t_{n+1}, from the current position, z_n. We here consider a water column of finite depth H (depth positive downwards), and a particle rising with a constant terminal speed v_b.

Step 1: Displace particle randomly

$$z_n' = z_n + \xi(z_n). \tag{4a}$$

Step 2: Reflect from boundaries

$$z_n'' = \begin{cases} -z_n' & \text{if} \quad z_n' < 0 \\ 2H - z_n' & \text{if} \quad z_n' > H \\ z_n' & \text{otherwise.} \end{cases} \tag{4b}$$

Step 3: Rise due to buoyancy

$$z_n''' = z_n'' - v_b\Delta t. \tag{4c}$$

Step 4: Set depth to 0 if above surface

$$z_{n+1} = \begin{cases} 0 & \text{if} \quad z_n''' \le 0 \\ z_n''' & \text{otherwise.} \end{cases} \tag{4d}$$

Depending on the application, a particle that reaches the surface in Step 4 may either remain in the water column, at a depth of 0 m, or it may be removed from the water and considered "surfaced". For an oil spill model, the latter would be the case, corresponding to the droplet merging with a continuous surface slick. It would then take energy in the form of breaking waves to re-introduce surfaced oil into the water column. In that case, a fifth step is also carried out at each timestep:

Step 5: If a particle is considered surfaced, it is resuspended with probability $p = 1 - \mathrm{e}^{-\Delta t/\tau}$, in which case it is assigned a random depth between $z = 0$ and $z = L$.

Note that in the case of slick-forming particles, Steps 1–4 are applied to all particles in the water column (*i.e.*, those particles that *are not* part of the surface slick), while Step 5 is applied to all particles that *are* part of the slick.

2.2. Eulerian model

The ADR equation describes the time-development of the concentration of a chemical or biological species affected by diffusive, advective and reactive processes. This may be expressed mathematically in the form of a partial differential equation (PDE),

$$\frac{\partial c}{\partial t} = \nabla\cdot(K\nabla c) - \nabla\cdot(\mathbf{v}c) + S, \tag{5}$$

where c is the concentration of species, K is the diffusivity, $\mathbf{v}$ is the velocity, and S is the reaction term.

[3] Note that breaking waves will of course also influence the behaviour of non-slick-forming particles, such as fish eggs. However, we have chosen to include this effect for slick-forming particles only, as it is far more important in this case, as can be seen by comparing the steady-state results of the three case studies in Section 3.

For the investigation of the vertical movement of particles (*e.g.*, oil droplets) in the water column, Eq. (5) may be simplified to one spatial dimension, that is, along the z-axis (depth positive downwards). The diffusivity is considered to be spatially dependent, that is, $K(z)$ in the vertical case. Similarly, the advection velocity, which in this case describes the rising of the individual particles due to buoyancy, may also be spatially dependent, *i.e.*, $v(z)$, to allow particles to stop at the surface and/or bottom boundaries of the water column. Furthermore, the reaction term may be considered dependent on position and concentration. Consequently, Eq. (5) becomes:

$$\frac{\partial c(z,\,t)}{\partial z} = \frac{\partial}{\partial z}\left(K(z)\frac{\partial c(z,\,t)}{\partial z}\right) - \frac{\partial}{\partial z}(v(z)c(z,\,t)) + S(z,\,c(z,\,t)), \tag{6}$$

where $c(z,t)$ represents the concentration of material, $K(z)$ is the spatially dependent diffusivity, $v(z)$ is the spatially dependent velocity and $S(z,c(z,t))$ is the source term.

2.2.1. Boundary conditions

In our Eulerian model, we have chosen to treat the transition of oil from the water column to the surface slick via the boundary conditions at the surface. An alternative is to model this process as a loss-term (also known as a sink), whereby oil near the surface is removed from the water column at some rate (see, *e.g.*, Ramírez et al. (2018), Tkalich and Chan (2002)). However, the use of a sink term requires the introduction of some length scale that determines what is meant by "close to the surface". For the Eulerian model, this could be a grid cell, but for the Lagrangian model, no such convenient length scale exists. Modelling the transition from subsurface to surface via the boundary conditions, on the other hand, gives a natural comparison between the Eulerian and Lagrangian schemes, as the concept of "reaching the surface" arises naturally in both models.

For the examination of oil droplets, which rise toward the surface and create an oil slick, we propose a partially absorbing boundary condition, where only the advective flux is allowed to transport particles out of the domain through the surface boundary located at $z = 0$, while we demand that the diffusive flux be zero at the boundary. This is equivalent to Steps 2 and 4 in the particle model, where we reflect a particle that has been placed above the surface due to the random walk, and consider a particle "surfaced" if it crosses the boundary due to buoyancy.

Writing the total flux as the sum of the advective flux and the diffusive flux, $j_T = j_A + j_D$, we may write the above boundary condition as

$$\begin{aligned} j_T|_{z=0} &= (j_A + j_D)|_{z=0} \\ &= \left(v(z)c(z,\,t) - K(z)\frac{\partial c(z,\,t)}{\partial z}\right)\Bigg|_{z=0} = v(z)c(z,\,t)\Big|_{z=0}, \end{aligned} \tag{7}$$

which then can be simplified to the following Neumann boundary condition for the diffusive flux at the surface:

$$j_D|_{z=0} = K(z)\frac{\partial c(z,\,t)}{\partial z}\Bigg|_{z=0} = 0. \tag{8}$$

We note that if the velocity $v(z = 0)$ at the surface boundary is set to zero, the boundary condition reduces to a fully reflective boundary, since there will be no advection through the surface. This may for instance be used in the simulation of particles that do not create a slick at the surface (*e.g.*, buoyant fish eggs or microplastics).

In a similar manner, and to ensure that no particles leave the domain at the bottom boundary, located at $z = H$, we propose a reflective boundary condition, where the total flux is zero, *i.e.*,

$$j_T|_{z=H} = (j_A + j_D)|_{z=H} = \left(v(z)c(z,\,t) - K(z)\frac{\partial c(z,\,t)}{\partial z}\right)\Bigg|_{z=H} = 0, \tag{9}$$

which takes the form of a Robin boundary condition, that is, a combination of a Dirichlet and a Neumann boundary condition.

2.2.2. Reaction term for resuspension of oil from an oil slick

Let C_{tot} be the total amount of material considered in the simulation. Assuming that we consider a system with a finite depth, H, and we start out at time t_0 with all the material being submerged (*i.e.*, nothing on the surface), we have

$$C_{tot} = \int_0^H c(z,\,t_0)\,\mathrm{d}z. \tag{10}$$

Then, at any time, t_n, the amount of material in the surface slick, $C_{slick}(t_n)$, can be found as

$$C_{slick}(t_n) = C_{tot} - \int_0^H c(z,\,t_n)\,\mathrm{d}z. \tag{11}$$

In our model, oil from the surface slick may be resuspended as droplets by assuming an exponential decay of the amount of oil at the surface, with a decay rate $\lambda = 1/\tau$, where τ is the corresponding lifetime. This is equivalent to submerging a constant fraction of the surface slick at every timestep, where that fraction is given by

$$p = 1 - \mathrm{e}^{-\Delta t/\tau}. \tag{12}$$

Hence, the amount of oil resuspended during timestep n is

$$pC_{slick}(t_n), \tag{13}$$

and the corresponding source term is given by

$$S(z,\,c(z,\,t_n)) = \begin{cases} p\dfrac{C_{slick}(t_n)}{L\Delta t} & \text{if} \quad z \le L, \\ 0 & \text{otherwise}, \end{cases} \tag{14}$$

where Δt is the timestep of the model. In this case, the resuspended material is distributed uniformly throughout the upper part of the water column, down to the depth L (see also Section 2.1, Step 5).

2.2.3. Numerical solution method for the advection-diffusion-reaction equation

To solve Eq. (6), a finite volume method (FVM) was used. The z-axis was discretised into control volumes, or cells, of a constant size Δz. Then, the diffusive fluxes through the cell faces were approximated by a second-order central difference of the two adjacent cells. Moreover, *flux limiting* was used to approximate the advective fluxes as a first-order upwind flux with a (higher-order) correction depending on a limiter function (Hundsdorfer, 2003, pp. 66–67). The flux limiting was performed with a QUICK (quadratic upstream interpolation for convective kinetics) limiter function, yielding second-order spatial accuracy (see, *e.g.*, Versteeg (2007, pp. 170, 178)). Finally, the finite volume scheme was discretised in time according to Eq. (1) and integrated by the Crank-Nicolson method (implicit trapezoidal rule) in order to achieve second-order accuracy in time and favourable unconditional stability (see, *e.g.*, Versteeg (2007, pp. 247–248)). See Appendix A for further details.

3. Case studies

In this section, we present and discuss the results of three example cases. In each case, we present the solution as calculated both by the Eulerian grid model and the Lagrangian particle model, to demonstrate that they give equivalent results. For both models, we consider a finite water depth of $H = 40$ m. For the Eulerian model, a spatial discretisation of $\Delta z = 0.04$ m was used, and a timestep of $\Delta t_E = 1$ s. For the Lagrangian particle model, $N_p = 960{,}000$ particles were used, and a timestep of $\Delta t_L = 0.01$ s. The same numerical parameters were used for all three case studies. See Appendix B for details on the choice of numerical parameters for the particle model.

In order to directly compare the results, both models were used to calculate concentrations. For the Eulerian model, the initial

concentration was in all cases a Gaussian concentration profile centred at $z = \mu_0 = 20$ m, with a standard deviation of $\sigma_0 = 2$ m. Hence we have

$$C_{tot} = \int_0^H \frac{1}{\sqrt{2\pi\sigma_0^2}} \exp\left(-\frac{(z-\mu_0)^2}{2\sigma_0^2}\right) \mathrm{d}z \approx 1, \tag{15}$$

where the integral can for practical purposes be considered equal to 1.

To calculate equivalent concentrations from the particle model, the initial positions of the particles were drawn from a Gaussian random distribution with the same properties as the above ($\mu_0 = 20$ m, $\sigma_0 = 2$ m). The z-axis on the interval $z = 0$ to $z = H$ was divided into $N_b = 1000$ bins, giving a bin size equal to the spatial resolution, $\Delta z = 0.04$ m, of the Eulerian model. The particle count in each bin was then converted to a normalised concentration by dividing by $N_p \Delta z$. Note that during the simulation, the depth of a particle can have any value. The concentration bins are only introduced as a means to calculate concentrations, and do not affect the particle positions. After calculating the binned concentrations, these were averaged over 100 consecutive timesteps, to get profiles that represent average conditions over the same interval as the timestep of the Eulerian model, $\Delta t_E = 1$ s.

We have considered two different diffusivity scenarios. One where the diffusivity is a constant, $K = 3 \cdot 10^{-3}$ m^2/s, and one where it varies with depth. For ease of implementation, we have chosen to consider a variable profile that is given by an analytical expression. Following Visser (1997), we use a diffusivity, $K(z)$, given by

$$K(z) = K_0 + K_1 z \mathrm{e}^{-\alpha z}, \tag{16a}$$

$$K_0 = 10^{-3}\ \mathrm{m^2/s}, \quad K_1 = 6{\cdot}10^{-3}\ \mathrm{m/s}, \quad \alpha = 0.5\ \mathrm{m^{-1}} \tag{16b}$$

which approximates a wind-forced surface boundary layer with a mixing layer depth of approximately 10 m. The diffusivity profiles are shown in Fig. 1.

3.1. Case 1: Fish eggs

We consider here a case where we have buoyant particles, with a rise velocity of 6 mm/s. This corresponds approximately to the rise velocity of fish eggs with a density of 1.01 kg/L, and a size of 1 mm. In this case, the boundary condition at the surface is zero flux in both advection and diffusion, thus describing particles that do not form a slick at the surface (see discussion in Sections 2 and 2.1).

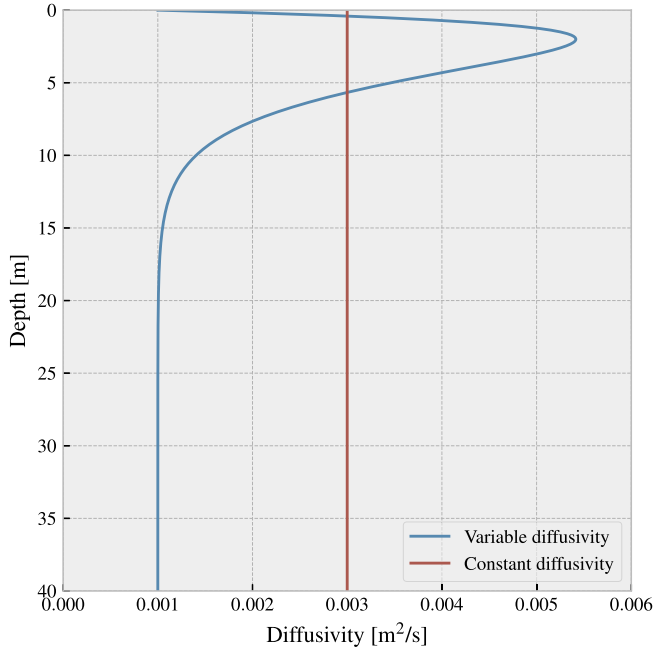

Fig. 1. Diffusivity profiles used in the case studies: One constant profile, and one profile where diffusivity is a function of depth, as given by Eq. (16).

We have simulated this scenario with the two different diffusivities shown in Fig. 1, *i.e.*, a constant diffusivity of $K = 3 \cdot 10^{-3}$ m^2/s, and a variable diffusivity given by Eqs. (16). In Fig. 2, the results obtained with constant diffusivity are presented. Concentration profiles are shown in the left panel, calculated both with the Lagrangian particle model described in Section 2.1, and with the Eulerian model described in Section 2.2. Concentrations at five different times are shown, with the five coloured lines showing the results of the Lagrangian model, and the corresponding dashed black lines showing the results of the Eulerian scheme. We find that the two models give very similar predictions. It is furthermore observed that the concentration profiles at 2, 3 and 4 h appear identical. This is because after about 2 h, a steady state is reached, where the upward drift due to buoyancy is exactly balanced by a downwards displacement caused by diffusion in the presence of a reflecting boundary (*i.e.*, the surface).

In the right panel of Fig. 2, concentration in the topmost bin (*i.e.*, the interval from $z = 0$ to $z = \Delta z = 0.04$ m) is shown as a function of time, again for both models, with the Lagrangian particle model results shown as a continuous blue line and the Eulerian grid model as a dashed black line. That the system reaches a steady state is clearly visible, as the concentration in the topmost bin reaches a constant level after about 2 h. Even after the steady state is reached, we observe that the concentration in the topmost bin fluctuates in the particle model, due to the inherent randomness of the random walk scheme. However, the time-averaged concentrations in the top bin, over the interval from 5 to 6 h, is 1.92268 m^{-1} for the particle model and 1.92170 m^{-1} for the grid model, which is a discrepancy of 0.053% between the two models.

For the special case considered here, with constant rise speed and diffusivity, and completely reflecting boundary, the PDE for the concentration profile (Eq. (6)) has an analytical solution given by

$$C(z) = C_0 \mathrm{e}^{-z\frac{v_b}{K}}, \tag{17}$$

where K is the diffusivity, v_b is the constant rise speed and C_0 is the concentration at the surface. By using that the integral of the concentration over the entire water column should be unity, we find the following analytic solution for the normalised average concentration in the top bin:

$$\frac{1}{\Delta z} \frac{\int_0^{\Delta z} \mathrm{e}^{-zv_b/K}\,\mathrm{d}z}{\int_0^H \mathrm{e}^{-zv_b/K}\,\mathrm{d}z} \approx 1.92209134033411. \tag{18}$$

Strictly speaking, the above expression is only approximate, as Eq. (17) only holds for infinite water depth. However, due to the rapid exponential falloff it is accurate to about 36 decimal places.

In Fig. 3, similar results are shown for the same case of buoyant particles with a completely reflecting boundary, but this time with a variable diffusivity given by Eqs. (16). Again, the left panel shows concentration profiles at five different times, and the right panel shows the concentration in the top bin for both models. We observe that also in this case a steady state is reached. However, we note that this time there is a visible discrepancy in the predicted steady-state concentration of the topmost cell (Fig. 3, right panel), where the particle scheme predicts a concentration of 2.25304 m^{-1}, while the grid model predicts 2.23698 m^{-1} (in both cases an average over the interval from 5 to 6 h is taken). This difference of about 0.7% is presumably caused by an artificial build-up of particles near the boundary, which occurs in the reflection step when the diffusivity profile has a non-zero derivative approaching the boundary (see Ross and Sharples (2004) and Section 4). The comparison of the steady-state predictions is summarised in Table 1, and the observed discrepancy in the case of variable diffusivity will be analysed and discussed further in Section 4.

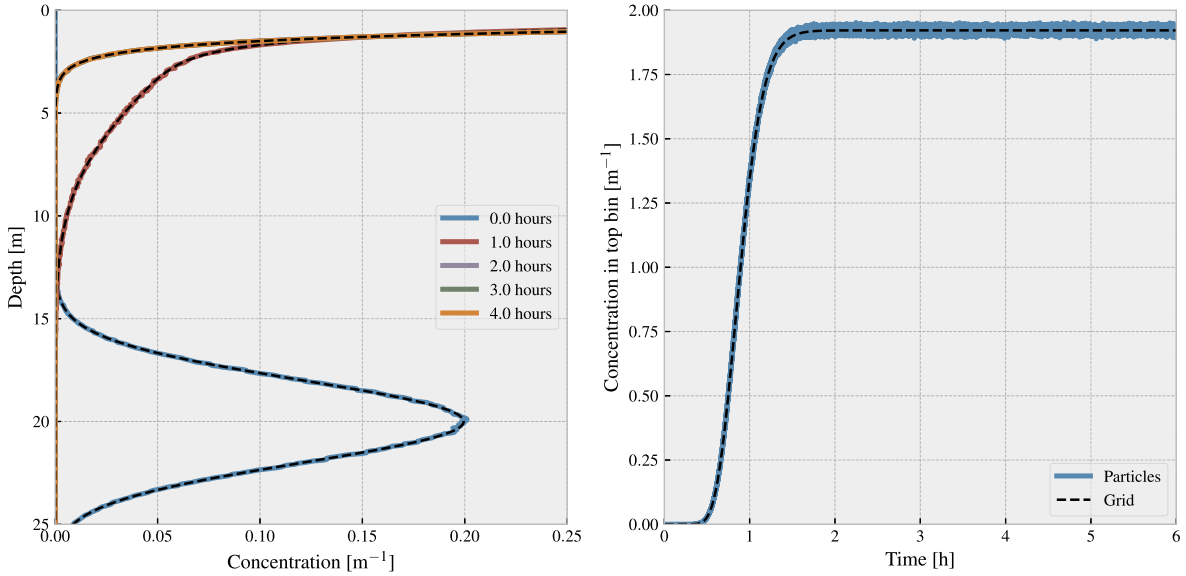

Fig. 2. Case 1: fish eggs, constant diffusivity. In the left panel, concentration profiles are shown for several different times, for an initial distribution of a Gaussian centred at a depth of 20 m (the blue line). The continuous coloured lines show the results for the Lagrangian model, while the dashed black lines show the corresponding timesteps for the Eulerian model. In the right panel, concentration in the top bin ($0 \leq z < \Delta z$) is shown as a function of time, for both models.

3.2. Case 2: Oil droplets

In this case, we consider particles with a rise velocity of 3 mm/s, which corresponds approximately to oil droplets with a density of 0.9 kg/L, and a size of 0.25 mm. Note that this value was somewhat arbitrarily chosen as an example, and should not be seen as representative for oil spills in general.

The boundary at the surface is treated as reflective in diffusion, but absorbing in advection. This represents oil droplets being absorbed into the surface slick if they reach the surface due to buoyancy, but not if they reach the surface due to diffusion (see details in Section 2). In this case, we present results for the variable diffusivity profile only (see Eqs. (16)).

The results of the simulation are shown in Fig. 4, again with concentration profiles for different times shown in the left panel. The results from the Lagrangian model are shown as continuous coloured lines, while the predictions of the Eulerian model are shown for the

Table 1
Results for Case 1. Calculated average steady-state concentration in the top bin (*i.e.*, $0 \leq z < \Delta z = 0.04$ m). For both numerical schemes, an average over the interval from 5 to 6 h is taken.

	Constant diffusivity	Variable diffusivity
Analytical solution	1.92209	-
Particle model	1.92268	2.25304
Grid model	1.92170	2.23698
Difference between particle and grid	0.053%	0.72%

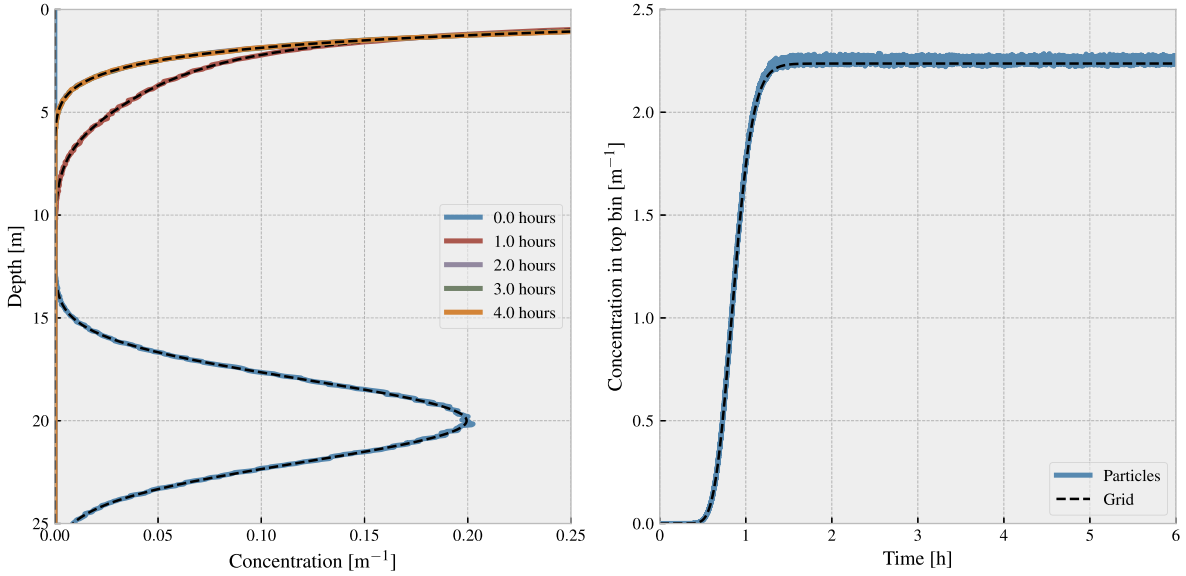

Fig. 3. Case 1: fish eggs, variable diffusivity. In the left panel, concentration profiles are shown for several different times, for an initial distribution of a Gaussian centred at a depth of 20 m (the blue line), and a diffusivity profile given by Eqs. (16). The continuous coloured lines show the results for the Lagrangian model, while the dashed black lines show the corresponding timesteps for the Eulerian model. In the right panel, concentration in the top bin ($0 \leq z < \Delta z$) is shown as a function of time, for both models.

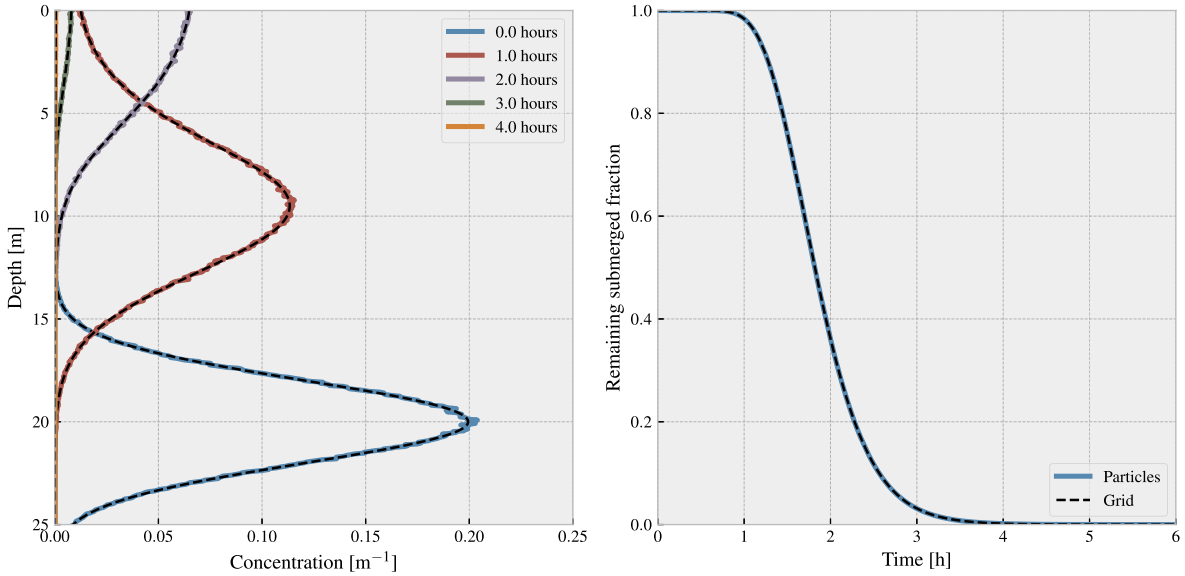

Fig. 4. Case 2: oil droplets, variable diffusivity. In the left panel, concentration profiles are shown for several different times, for an initial distribution of a Gaussian centred at a depth of 20 m (the blue line). The continuous coloured lines show the results for the Lagrangian model, while the dashed black lines show the corresponding timesteps for the Eulerian model. In the right hand panel, the submerged fraction is shown as a function of time.

same times as dashed black lines. In the right panel, the fraction of material that remains in the water column (*i.e.*, the fraction that has not been absorbed into the surface slick) is shown.

We again observe that the two different models give very similar predictions, both for the concentration profiles and for the amount of oil remaining in the water column as a function of time. In this case, the steady-state solution is that all the material has settled on the surface, with no droplets left in the water column.

3.3. Case 3: Oil droplets with resuspension

In the final case, we again consider particles with a rise velocity of 3 mm/s, which corresponds approximately to oil droplets with a density of 0.9 kg/L, and a size of 0.25 mm. Note again that this value was somewhat arbitrarily chosen as an example, and should not be seen as representative for oil spills in general. Furthermore, the boundary at the surface is treated as reflective in diffusion, but absorbing in advection. This represents oil droplets being absorbed into the surface slick if they reach the surface due to buoyancy. In contrast to Case 2, however, this time the model includes resuspension. At each timestep, a constant fraction $p = 1 - \mathrm{e}^{-\Delta t/\tau}$ of the surface slick is resuspended into the water column. This is equivalent to exponential decay of the amount of surface oil, at a rate corresponding to a lifetime, τ, at the surface, where we have arbitrarily chosen $\tau = 500$ s. The resuspended oil is evenly distributed throughout the interval from $z = 0$ to $z = L$, where the entrainment depth was also somewhat arbitrarily set to $L = 1$ m. As noted in Section 2, the entrainment depth and rate, as well as the droplet size distribution of the entrained oil, will in general depend on the wave state and the properties of the oil (see, *e.g.*, Delvigne and Sweeney (1988), Johansen et al. (2015), Li et al. (2017)). However, these

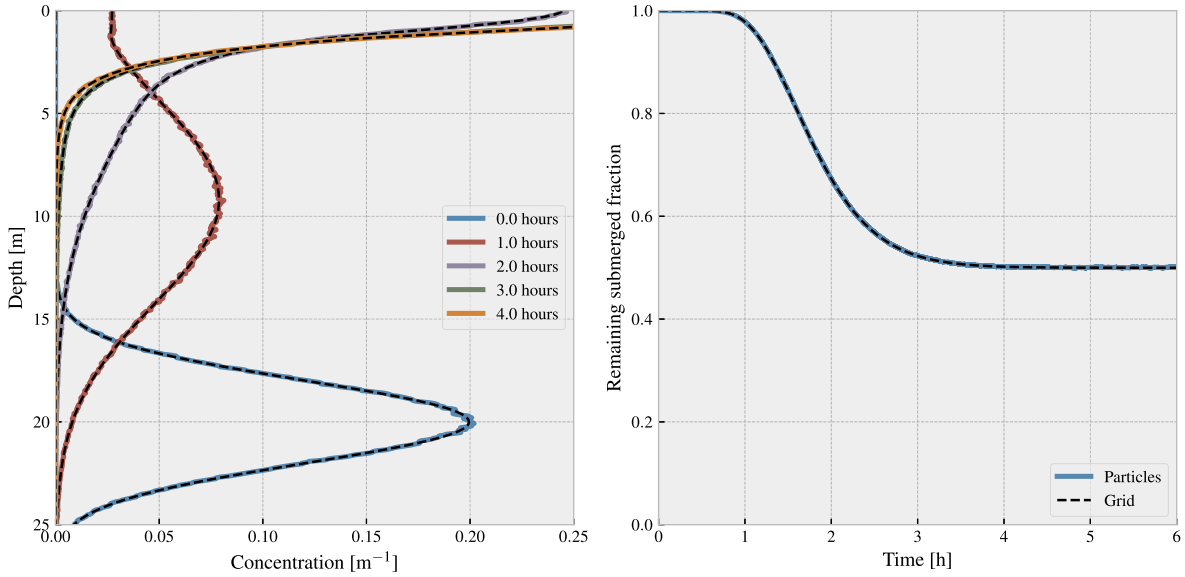

Fig. 5. Case 3: oil droplets with resuspension, constant diffusivity. In the left panel, concentration profiles are shown changing over time, for an initial distribution of a Gaussian centered at a depth of 20 m (the blue line). The continuous coloured lines show the results for the Lagrangian model, while the dashed black lines show the corresponding timesteps for the Eulerian model. In the right hand panel, the submerged fraction is shown as a function of time.

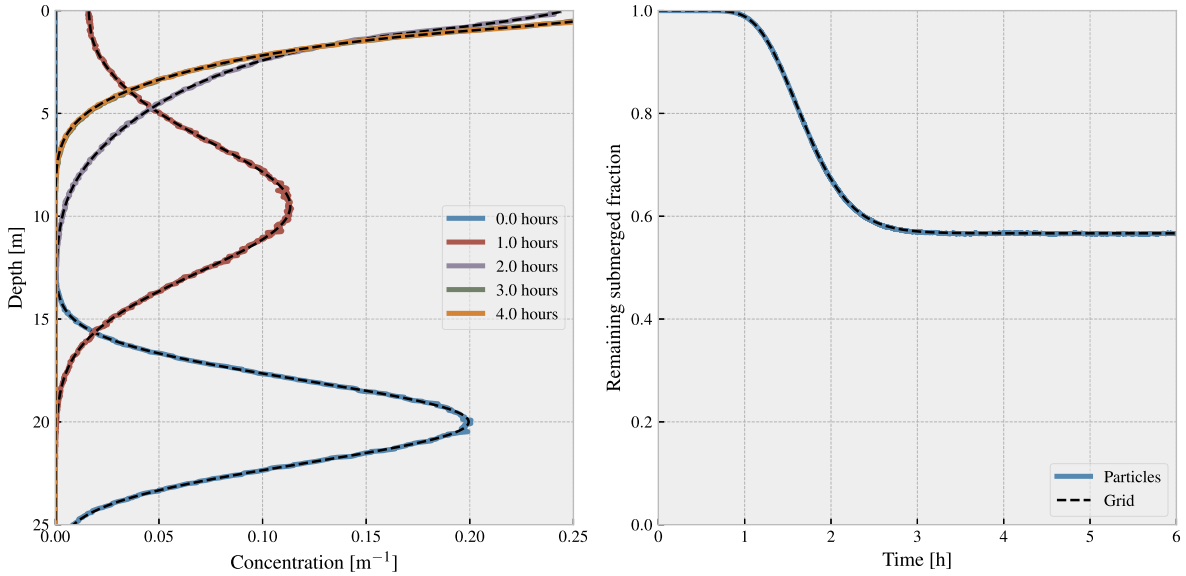

Fig. 6. Case3: oil droplets with resuspension, variable diffusivity. In the left panel, concentration profiles are shown changing over time, for an initial distribution of a Gaussian centred at a depth of 20 m (the blue line), and a diffusivity profile given by Eqs. (16). The continuous coloured lines show the results for the Lagrangian model, while the dashed black lines show the corresponding timesteps for the Eulerian model. In the right hand panel, the submerged fraction is shown as a function of time.

Table 2
Results for Case 3. Calculated submerged fraction at steady state. For both numerical schemes, an average over the interval from 5 to 6 h is taken.

	Constant diffusivity	Variable diffusivity
Analytical solution	-	-
Particle model	0.5005	0.5659
Grid model	0.4998	0.5667
Difference between particle and grid	0.14%	0.14%

complications do not directly affect the discussion of the boundary conditions, and are thus outside the scope of the current investigation.

This case has also been simulated with both constant and variable diffusivity. The results of the simulations with constant diffusivity are shown in Fig. 5, in the same way as for Case 2, *i.e.*, with concentration profiles in the left panel, and remaining submerged fraction as a function of time in the right panel. We again observe that the two different models give very similar predictions, both for the concentration profiles and for the amount of oil remaining in the water column as a function of time. In this case a steady state is reached, where a significant fraction of the material remains submerged. This state is reached after about 4 h. At the steady state, the upwards drift due to buoyancy is exactly balanced by the combined downwards motion due to resuspension, and diffusion in the presence of a reflecting boundary. We observe that the two different models predict essentially the same time-development of the remaining submerged fraction, as well as very similar steady-state level. At steady-state, the predicted submerged fraction is 0.5005 in the particle model, and 0.4998 in the grid model, a discrepancy of about 0.14%. Here, the average over the interval from 5 to 6 h was used.

The same situation as the above has been simulated with the variable diffusivity profile given by Eqs. (16), and the results are shown in Fig. 6. Again, concentration profiles are shown in the left panel, and submerged fraction as a function of time in the right panel. A steady state is reached also in this situation, and after about 3–4 h the submerged fraction remains approximately constant. At steady state, the predicted submerged fraction is 0.5659 for the particle model, and 0.5667 for the grid model, where the average from 5 to 6 h has been taken in both cases. The results are summarised in Table 2.

4. Discussion

In this section, we discuss some technical details of the reflecting boundary in the Lagrangian particle model, as well as our reasons for choosing to model the removal of oil from the water column via the boundary conditions in the Eulerian scheme.

4.1. Boundary treatment in Lagrangian models

We mentioned initially that there are a number of somewhat subtle details that must be taken into account in formulating a particle model. First among these are the correct formulation of the random walk, to avoid unphysical transport away from regions of high diffusivity. Random walk schemes are essentially numerical integration methods for stochastic differential equations, and there are a range of available methods at different orders of accuracy. For a detailed survey of several alternative methods, see, *e.g.*, Gräwe (2011), Gräwe et al. (2012), as well as specialist literature such as Kloeden and Platen (1992).

In this paper, we have chosen to use the Visser scheme (see Visser (1997) for details). While higher-order methods may allow longer timesteps, and better handle sharp transitions in diffusivity, they will typically formulate the transport process as a single step that includes both random displacement and drift (in this case, rise due to buoyancy). The Visser scheme, on the other hand, allows us to handle the drift as a separate step. This is convenient when we want to split the advection and diffusion steps to treat the boundary at the surface as reflecting in diffusion and absorbing in advection.

On the topic of reflecting boundaries in spatially variable diffusion, Ross and Sharples (2004) have demonstrated that simple reflection is not strictly correct. In our case, when using the Visser scheme with a reflecting boundary, and a diffusivity profile whose derivative does not go to zero at the boundary, one will observe a spurious increase in concentration of particles near the boundary[4]. The effect can however be made arbitrarily small by choosing a sufficiently short timestep. We

[4] Note that this effect is not unique to the Visser scheme, but may take a different shape with other schemes.

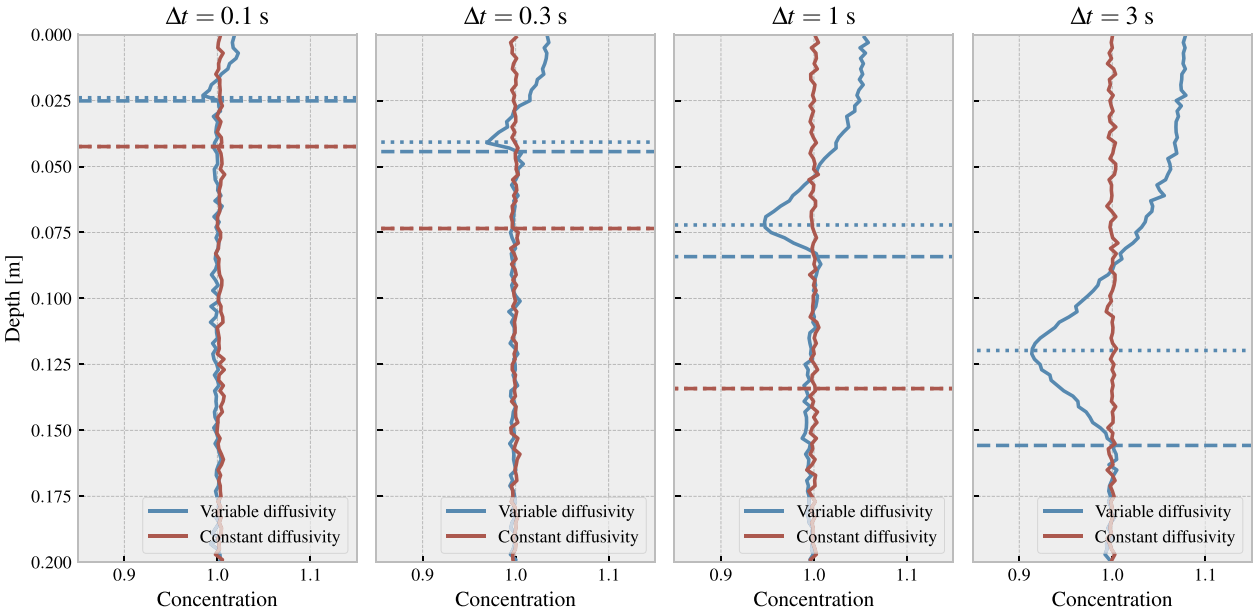

Fig. 7. Concentration profiles (arbitrary units), averaged over 12 h, shown for constant and variable diffusivity (see Eqs. (16)), and for four different timesteps, Δt. For each case, the depth h_1 is indicated by a dashed line, and h_2 by a dotted line (see Eq. (19)). For constant diffusivity, $h_1 = h_2$. Note that only the 20 cm closest to the boundary are shown.

demonstrate this with a numerical example.

As we have taken R in Eq. (2) to be uniformly distributed random numbers between -1 and 1, it is possible to calculate the maximum upwards and downwards displacements a particle can have, at any position. Inspired by Ross and Sharples (2004), we introduce the parameters h_1 and h_2 to describe the range of possible displacements of a particle situated exactly *at* the reflecting boundary. Here, h_1 is the maximum displacement of a particle moving away from the boundary, while h_2 is the maximum displacement of a particle moving into the boundary, followed by reflection (note that our definition of h_1 differs from Ross and Sharples (2004), while h_2 is the same). Hence, h_1 and h_2 for the boundary at the surface ($z = 0$) are in our case given by

$$h_1 = K'(0)\Delta t + \sqrt{6\Delta t K\left(0 + K'(0)\tfrac{\Delta t}{2}\right)}, \tag{19a}$$

$$h_2 = -K'(0)\Delta t + \sqrt{6\Delta t K\left(0 + K'(0)\tfrac{\Delta t}{2}\right)}. \tag{19b}$$

These parameters indicate the size of the region affected by the spurious concentrations.

As a numerical example, we consider a case with neutrally buoyant tracers, in a finite depth of 10 m, with the same diffusivity profiles as used earlier, *i.e.*, a constant $K = 3 \cdot 10^{-3}$ m^2/s, and a variable profile given by Eqs. (16). The diffusivity profiles are shown in Fig. 1. We employ an ensemble of $N_p = 200{,}000$ tracers, initially distributed in a uniform manner in the whole domain, and let the system develop for 12 h. The resulting concentrations, averaged over 12 h, are shown in Fig. 7, where the calculations have been performed with four different timesteps, Δt, and the concentrations have been calculated by normalised particle counts in $N_b = 5000$ bins. In principle, the tracers should remain well mixed, however, as can be seen this is not the case close to the boundary when the variable diffusivity profile is used.

In each panel of Fig. 7, the parameter h_1 has been indicated by a horizontal dashed line, while h_2 is indicated by a dotted line. We observe that for a constant diffusivity, $h_1 = h_2$, and there is no spurious concentration effect. For the variable profile, on the other hand, $h_1 \neq h_2$, and hence there is a region of higher concentration close to the boundary, followed by another region of reduced concentration. We observe from Eqs. (19) that the size of the region with spurious concentrations is dependent on the timestep, Δt, as well as on the behaviour of the diffusivity profile near the boundary. Note in particular that if $K'(z = 0) = 0$, the effect disappears (provided the timestep is sufficiently short, cf. Eq. (3)).

For our Case studies with variable diffusivity, which were carried out with the diffusivity profile given by Eqs. (16), and a timestep of $\Delta t = 0.01$ s, we find that

$$h_1 = 0.007806 \text{ m}, \quad h_2 = 0.007686 \text{ m}. \tag{20}$$

While these values are smaller than the bin size used to calculate concentrations (which was $\Delta z = 0.04$ m), we found in Case 1, when a variable diffusivity was used, a slightly increased prediction of the near-surface concentration (see Fig. 3, right panel), when the particle model is compared to the Eulerian model. The effect was not observed for constant diffusivity in Case 1. It was also not seen in Cases 2 and 3, where any spurious accumulation at the surface is continuously removed by the combined effect of upwards drift due to buoyancy and the absorbing boundary condition in advection. One might have expected an increase in concentration near the surface to lead to faster surfacing of the oil in Cases 2 and 3, but no indication of this is found at the timestep length used here.

4.2. Boundary treatment in Eulerian models

In the current study, we have chosen to describe the transition of oil from the water column to the surface slick via the boundary conditions in the Eulerian scheme. This is a natural way to describe the process, as a droplet joining the surface slick will pass through a boundary at the oil-water interface, and join the continuous oil phase. It also allows for a straightforward comparison between the Lagrangian and Eulerian schemes, as the concept of the boundary at the surface exists in both.

As previously mentioned, an alternative would be to formulate the disappearance of oil from the water column as a loss term, or sink, in the ADR equation. An example of such a formulation is found in Tkalich and Chan (2002), where the loss of oil to the surface slick is modelled by assuming the existence of a well-mixed layer near the surface, throughout which the oil concentration is constant. At each timestep, some fraction of the oil in this layer is lost to the surface, where this fraction is determined from the rise speed of the droplets, and the thickness of the well-mixed layer.

In our opinion, treating the surfacing of oil via the boundary conditions should be the preferred approach, as it does not require any assumptions about the existence of special layers. In formulating our Eulerian model, we have assumed that the transport and mixing of buoyant material in the water column can be described by the advection-diffusion equation, with the diffusivity given by an eddy diffusivity profile, and that the buoyant material can optionally leave the water column through its natural boundary at the surface, to form a continuous, floating slick.

5. Conclusion

We have analysed a Lagrangian particle model for vertical transport, mixing, surfacing and optionally resuspension of buoyant materials, such as oil droplets, microplastics and fish eggs. The Lagrangian model is compared to an Eulerian model based on direct numerical solution of the ADR equation. We have described how to treat the boundary at the surface in order to model materials that form a slick at the surface, such as oil, as well as non-slick-forming materials such as plastics and fish eggs. In particular, we demonstrate that treating the surface in the particle model as completely reflecting is equivalent to solving the ADR equation with a Robin boundary condition, ensuring no flux across the boundary. Moreover, we have demonstrated that treating the surface in the particle model as absorbing in advection, and reflecting in diffusion, gives the same results as solving the ADR equation with a Neumann boundary condition enforcing zero diffusive flux, while allowing an advective flux. We also consider the effect of entrainment of surface oil due to waves in both models, and again demonstrate that consistent results emerge.

While it is likely that many particle-based oil spill models use a similar approach to the one outlined in Section 2.1, an explicit description and analysis of the steps involved in surfacing has, to the best of our knowledge, never appeared in the literature. Furthermore, while most oil spill models are based on Lagrangian particle schemes, Eulerian oil spill models exist and are being developed (see, *e.g.*, Restrepo et al. (2015), Tkalich et al. (2003)), hence it is a point of some importance to have an understanding of how to formulate equivalent descriptions in the two schemes.

Acknowledgements

The authors would like to thank their colleagues for many an interesting discussion in the SINTEF CoffeeLab. The work has been performed partially under the project HPC-EUROPA3 (INFRAIA-2016-1-730897), with the support of the EC Research Innovation Action under the H2020 Programme; in particular, T.N. gratefully acknowledges the computer resources and technical support provided by the EPCC.

Appendix A. Details on the implementation of the Eulerian finite volume method

In FVMs, the partial differential equation is transformed to integral form by integrating over a control volume Ω_j corresponding to cell j. Considering Eq. (6), the volume integrals on the right-hand side may then be rewritten to surface integrals over the boundary of the control volume through the divergence theorem. By applying the Leibniz integral rule on the left-hand side to change the order of the spatial integral and the differentiation with respect to time, the average concentration in control volume Ω_j, $\bar{c}_j$, may be defined. Similarly, on the right-hand side, the average reaction term in the control volume, $\bar{S}_j$, is found by integration.

Since only flow in the vertical z-direction is considered, the left-hand side of Eq. (6) reduces to the change of the cell-average concentration per unit of time in the control volume with the grid spacing $\Delta z_j = z_{j+\frac{1}{2}} - z_{j-\frac{1}{2}}$. Moreover, the right-hand side is given by the difference of the diffusive and advective fluxes at the bottom and top faces of the control volume, $z_{j+\frac{1}{2}}$ and $z_{j-\frac{1}{2}}$ (depth positive downwards), respectively, with the addition of the cell-average source term in the control volume with the grid spacing Δz_j. Thus, the integral form of Eq. (6) reads:

$$\Delta z_j \frac{\mathrm{d}\bar{c}_j}{\mathrm{d}t} = \left(K\frac{\partial c}{\partial z}\right)_{j+\frac{1}{2}} - \left(K\frac{\partial c}{\partial z}\right)_{j-\frac{1}{2}} - (vc)_{j+\frac{1}{2}} + (vc)_{j-\frac{1}{2}} + \Delta z_j \bar{S}_j, \tag{A.1}$$

which is noted to be an exact equation. Now, the concentration is assumed to be constant within each control volume, such that the cell-averages, $\bar{c}_j$ and $\bar{S}_j$ may be approximated by the values located at the cell centres, z_j, that is, c_j and S_j, respectively. Assuming a constant grid spacing Δz, the z-axis is thus discretised into NJ equidistant control volumes (or cells). A similar derivation may, *e.g.*, be found in Versteeg (2007, pp. 243–246).

Considering the cell adjacent to the surface boundary, notated as $j = 0$, the insertion of the absorbing surface boundary condition of Eq. (8) into Eq. (A.1) causes the diffusive flux over the surface to vanish. Thus, Eq. (A.1) reduces to

$$\Delta z \frac{\mathrm{d}c_0}{\mathrm{d}t} = \left(K\frac{\partial c}{\partial z}\right)_{\frac{1}{2}} - (vc)_{\frac{1}{2}} + (vc)_{-\frac{1}{2}} + \Delta z S_0, \tag{A.2}$$

where $j = -\frac{1}{2}$ corresponds to the surface boundary. Moreover, as noted in Section 2.2.1, if the velocity over the surface is zero, the advective flux over the surface also vanishes, making the surface a reflecting boundary.

Similarly, in the cell adjacent to the bottom boundary, *i.e.*, $j = NJ - 1$, inserting the reflecting boundary condition from Eq. (9) into Eq. (A.1) causes both the diffusive and advective fluxes over the bottom boundary to disappear. Hence, Eq. (A.1) reduces to

$$\Delta z \frac{\mathrm{d}c_{NJ-1}}{\mathrm{d}t} = \left(K\frac{\partial c}{\partial z}\right)_{NJ-\frac{1}{2}} - \left(K\frac{\partial c}{\partial z}\right)_{NJ-\frac{3}{2}} - (vc)_{NJ-\frac{1}{2}} + (vc)_{NJ-\frac{3}{2}} + \Delta z S_{NJ-1}, \tag{A.3}$$

where $j = NJ - \frac{1}{2}$ corresponds to the bottom boundary.

In Eq. (A.1), the diffusive fluxes at the cell faces were approximated by a second-order central difference of the two adjacent cells (see, *e.g.*, Versteeg (2007, p. 117)). That is, on the form

$$\left(K\frac{\partial c}{\partial z}\right)_{j+\frac{1}{2}} \approx K_{j+\frac{1}{2}} \frac{c_{j+1} - c_j}{z_{j+1} - z_j} = K_{j+\frac{1}{2}} \frac{c_{j+1} - c_j}{\Delta z}, \tag{A.4}$$

where the diffusivity $K_{j+\frac{1}{2}}$ is determined on the cell faces either explicitly by an analytic expression, or by an arithmetic or harmonic mean in the case of a discrete diffusivity.

For the advective fluxes, however, it is noted that linear numerical schemes of second-order accuracy and higher are known to yield numerical oscillations for *advection-dominated* problems, that is, when the *cell Péclet number* $\mathrm{Pe} = \frac{|v|\,\Delta z}{K} \gg 1$, for non-smooth solutions (Hundsdorfer, 2003, pp.

66–67, 118–119). Consequently, in order to implement a more flexible higher-order numerical scheme (that is, higher than first-order, in this case) for advection, *flux limiting* was used to approximate the advective fluxes as a first-order upwind flux with a (higher-order) correction depending on a limiter function (Hundsdorfer, 2003, pp. 216–217; Versteeg, 2007, pp. 165–171). The approximation of the advective fluxes thus takes the form

$$(vc)_{j+\frac{1}{2}} \approx v^+_{j+\frac{1}{2}}\left(c_j + \frac{1}{2}\psi\left(\rho^+_{j+\frac{1}{2}}\right)(c_{j+1} - c_j)\right) + v^-_{j+\frac{1}{2}}\left(c_{j+1} - \frac{1}{2}\psi\left(\rho^-_{j+\frac{1}{2}}\right)(c_{j+1} - c_j)\right), \tag{A.5}$$

where $\psi(\rho^{\pm})$ is the limiter function determining the correction, and $\rho^{\pm}$ is given by

$$\rho^+_{j+\frac{1}{2}} = \frac{c_j - c_{j-1}}{c_{j+1} - c_j} \tag{A.6a}$$

$$\rho^-_{j+\frac{1}{2}} = \frac{c_{j+2} - c_{j+1}}{c_{j+1} - c_j}, \tag{A.6b}$$

i.e., the local ratio of the upwind gradient to the downwind gradient (Versteeg, 2007, pp. 167, 171–172; Hundsdorfer, 2003, p. 216). The flux limiting was done with a QUICK (quadratic upstream interpolation for convective kinetics) limiter function, given by

$$\psi(\rho) = \max\left[0, \min\left(2\rho, \frac{3+\rho}{4}, 2\right)\right], \tag{A.7}$$

where $\psi(\rho) = \frac{3+\rho}{4}$ corresponds to the QUICK scheme, and resulted in second-order accuracy (see, *e.g.*, Versteeg (2007, pp. 170, 178)).

According to Versteeg (2007, pp. 167–168), higher-order accuracy without oscillatory behaviour for non-smooth solutions is attained if the scheme is *monotonicity preserving, i.e.*, that it does not create local extrema and does not increase or decrease existing local maxima or minima, respectively. Such monotonicity-preserving schemes will have the property of being *total variation diminishing* (TVD), that is, that the total variation $TV(\phi) = \sum_{j=1}^{NJ} |\phi_j - \phi_{j-1}|$ does not increase over time (Versteeg, 2007, p. 168). As noted in Versteeg (2007, pp. 168-171), flux limiter functions were derived to satisfy a number of criteria which ensures that the resulting scheme is TVD and second-order accurate.

The scheme was discretised in time according to Eq. (1) and integrated by the Crank-Nicolson method (or implicit trapezoidal rule), given by

$$\frac{c_j^{n+1} - c_j^n}{\Delta t} = \frac{1}{2}F_j^n + \frac{1}{2}F_j^{n+1}, \tag{A.8}$$

where F corresponds to the right-hand side of Eq. (A.1) evaluated at time steps n and $n+1$. This was utilised in order to get second-order accuracy in time and favourable unconditional stability (Versteeg, 2007, pp. 247–248). By including the higher-order correction of the flux limiting as an additional source term, that is, as a *deferred correction* (see Versteeg (2007, pp. 163–164, 172)), the scheme may be written as a system of equations that must be solved for each time level $(n+1)$ by defining a tridiagonal matrix of coefficients. The tridiagonal system of equations was at each time level solved by the tridiagonal matrix algorithm (TDMA) or Thomas algorithm (see, *e.g.*, Pletcher (2013, pp. 150–151)). However, due to the nonlinearities appearing in the source term and the deferred correction, an iterative approach must be used to update the coefficients until an acceptable solution is found at the $(n+1)$ time level (see, *e.g.*, Pletcher (2013, p. 440)). It is noted in Hundsdorfer (2003, p. 232) that the implicit trapezoidal rule for a pure advection problem is TVD for Courant numbers $C = \frac{|v|\Delta t}{\Delta z} \leq 1$.

Appendix B. Details on the choice of timestep and number of particles

In a Lagrangian particle model, there are two main numerical parameters that control the accuracy: the timestep, Δt, and the number of particles, N_p. Ideally, the modelled result will converge to the correct solution (which may or may not be known), as Δt becomes smaller, and N_p becomes larger.

When using a particle method, each particle position constitutes a sample from the true distribution of positions. Hence, the random noise that is seen when using few particles is not a systematic error, but rather an indication that the sample distribution has not yet converged to the true distribution. For practical applications, this amounts to a random error in the modelled concentration field. The convergence with number of particles is $\propto 1/\sqrt{N_p}$, which means that increasing the number of particles by a factor 10 only reduces the error by a factor $1/\sqrt{10}$. The computational effort, on the other hand, increases linearly with N_p.

The scaling of the error with the timestep depends on the chosen random walk scheme. In this paper, we have used the Visser scheme, which has order of convergence 1, in the weak sense (Gräwe, 2011). Technically, this means that the error in the moments of the modelled distribution (as compared to the moments of the true distribution) will scale as Δt, for sufficiently small Δt (Kloeden and Platen, 1992, pp. 326–327). Higher-order random walk schemes exist, although many have the drawback that one must evaluate higher order derivatives of the diffusivity (see, *e.g.*, Gräwe (2011), Gräwe et al. (2012), Kloeden and Platen (1992)).

However, in the special case of constant drift and constant diffusivity, *i.e.*, for a stochastic differential equation (SDE) given by

$$\mathrm{d}z = a\ \mathrm{d}t + b\ \mathrm{d}W(t), \tag{B.1}$$

where a and b are constants, all schemes reduce to the Euler-Maruyama scheme (Maruyama, 1955; Pavliotis, 2014, page 146), given by

$$z_{n+1} = z_n + a\ \Delta t + b\ \Delta W, \tag{B.2}$$

where ΔW is a Gaussian random variable with mean $\langle \Delta W \rangle = 0$, and variance $\langle \Delta W^2 \rangle = \Delta t$. For this reason, we chose to use Case study 1 with constant diffusivity (see Section 3.1) to carry out a convergence test, in order to determine a suitable timestep and number of particles. As in the results for Case 1, we have calculated the average concentration in the top $\Delta x = 0.04$ m of the water column, using the particle method with different Δt and N_p. We then calculated the error in the modelled result by subtracting the analytical solution (see Eq. (18)).

In Fig. B.8, the results of the convergence test are shown. In the left hand panel, we have used $N_p = 19{,}200$. We observe that the error scales linearly with Δt, down to a relative error of about $3 \cdot 10^{-3}$. From this point, the error due to too few particles dominates, and there is no additional accuracy gained by reducing the timestep further. In the middle panel, with $N_p = 192{,}000$, we observe that increasing the number of particles by a factor 10 has improved the accuracy by a factor of about $1/\sqrt{10}$. In this case, improved accuracy with reduced timestep is seen down to an error of

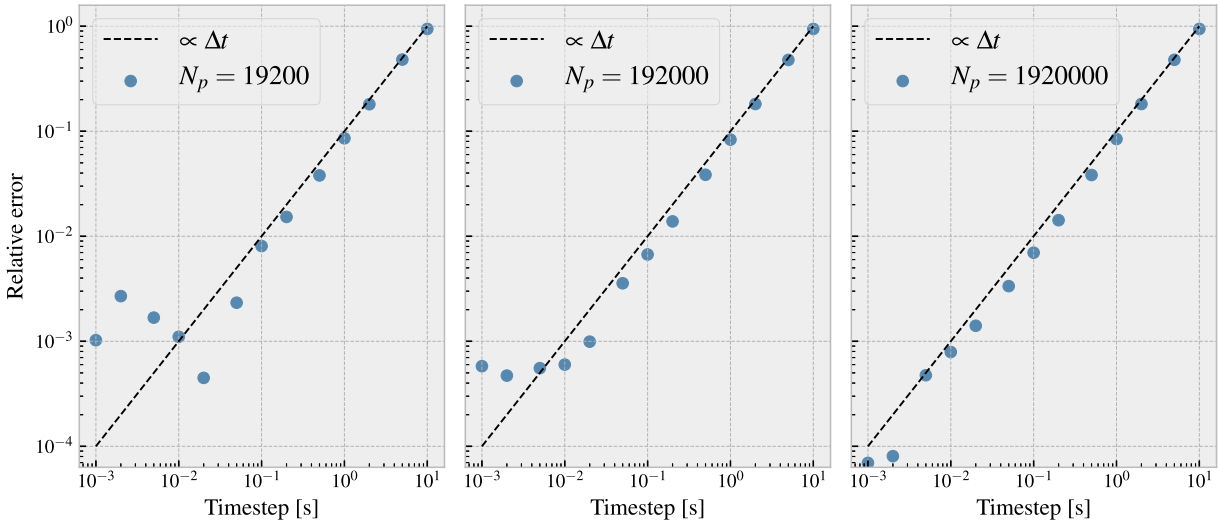

Fig. B.8. Relative error in the result from the particle model, compared to the analytical solution (see Case 1, Section 3.1 and Eq. (18)).

about 10^{-3}. Finally, in the right hand panel, the particle number is again increased tenfold, to $N_p = 1{,}920{,}000$. It is again clear that the increase in number of particles has led to an increased accuracy, and the timestep can profitably be decreased even further.

The convergence test indicates that with the numerical parameters used in the case studies ($N_p = 960{,}000$ and $\Delta t = 0.01$ s), we may reasonably expect a relative error of about $5 \cdot 10^{-4}$ for the case with constant diffusivity, which is what we see in Case 1. Note also that changing to a higher-order SDE scheme would *not* improve the accuracy when constant drift and diffusivity is used, as the correction terms in higher-order schemes typically contain derivatives of the drift and diffusivity, and the drift and diffusivity are the same no matter where they are evaluated (Gräwe, 2011; Gräwe et al., 2012; Kloeden and Platen, 1992).

A final point related to the number of particles is that this will depend on how the concentration field is calculated. One option is that one could use larger bins when counting particles to calculate the concentration. As larger bins will contain more particles, the results are then less suceptible to random fluctuations. The trade-off is a loss in resolution, in that features smaller than the bin size cannot be resolved. In this paper, we have chosen to use a fairly small bin size of $\Delta x = 0.04$ m, both for the Eulerian and the Lagrangian models. The intention was to facilitate a direct comparison, and to study the details of the behaviour near the boundary. In practical applications, such as in oil spill modelling, the bin size would more likely be on the scale of meters, rather than centimeters, and this would significantly reduce the need for a large number of particles.

Another commonly used approach, which may further reduce the need for large particle numbers, is to apply some kind of smoothing to the concentration field instead of using the box counts (which are equivalent to a histogram of particle positions). Lynch et al. (2014, Chapter 8) discuss some different options, including kernel estimators, also known as kernel density estimators (Silverman, 1986).

With a kernel estimator, the concentration field (in one dimension) is calculated as

$$C(z) = \frac{1}{N_p \lambda} \sum_{i=1}^{N_p} \kappa\left(\frac{z - z_i}{\lambda}\right), \tag{B.3}$$

where the sum is over particles, and z_i is the position of particle i. The kernel, $\kappa(z)$ can be any positive function that satisfies $\int \kappa(z)\, \mathrm{d}z = 1$, and λ is called the bandwidth. For the same number of particles, a kernel estimator can give a smoother and more accurate representation of the concentration field, compared to the box count approach. The results depend on both the kernel and the bandwith, the choices of which depend among other things on the number of particles (see, *e.g.*, Spivakovskaya et al. (2007)).

For the current study, we have chosen not to apply kernel estimators, as the focus of the investigation is on the boundary conditions, and not on the concentration field.

References

ASCE, 1996. State-of-the-art review of modeling transport and fate of oil spills. Journal of Hydraulic Engineering 122 (11), 594–609.

Ballent, A., Pando, S., Purser, A., Juliano, M., Thomsen, L., 2013. Modelled transport of benthic marine microplastic pollution in the Nazaré canyon. Biogeosciences 10 (12), 7957.

Brickman, D., Smith, P.C., 2002. Lagrangian stochastic modeling in coastal oceanography. Journal of Atmospheric and Oceanic Technology 19 (1), 83–99.

Castano-Primo, R., Vikebø, F.B., Sundby, S., 2014. A model approach to identify the spawning grounds and describing the earlylife history of Northeast Arctic haddock (Melanogrammus aeglefinus). Ices Journal of Marine Science 71 (9), 2505–2514.

Dagestad, K.-F., Röhrs, J., Breivik, O., Ådlandsvik, B., 2018, Apr. OpenDrift v1.0: a generic framework for trajectory modelling. Geosci. Model Dev. (1991-9603) 11 (4), 1405–1420. https://doi.org/10.5194/gmd-11-1405-2018.

De Dominicis, M., Pinardi, N., Zodiatis, G., Lardner, R., 2013. MEDSLIK-II, a Lagrangian marine surface oil spill model for short-term forecasting – part 1: Theory. Geoscientific Model Development 6 (6), 1851–1869.

Delvigne, G., Sweeney, C., 1988. Natural dispersion of oil. Oil and Chemical Pollution (0269-8579) 4 (4), 281–310. https://doi.org/10.1016/S0269-8579(88)80003-0.

Elliott, A.J., 1986, May. Shear diffusion and the spread of oil in the surface layers of the North Sea. Deutsche Hydrografische Zeitschrift (0012-0308, 1616-7228) 39 (3), 113–137. https://doi.org/10.1007/BF02408134.

Fox, C.J., McCloghrie, P., Nash, R.D., 2009. Potential transport of plaice eggs and larvae between two apparently self-contained populations in the Irish Sea. Estuarine, Coastal and Shelf Science 81 (3), 381–389.

French-McCay, D.P., 2009. Oil spill impact modeling: development and validation. Environmental Toxicology and Chemistry 23 (10), 2441–2456. https://doi.org/10.1897/03-382.

García-Martínez, R., Flores-Tovar, H., 1999. Computer modeling of oil spill trajectories with a high accuracy method. Spill Science & Technology Bulletin 5 (56), 323–330.

Gräwe, U., 2011. Implementation of high-order particle-tracking schemes in a water column model. Ocean Modelling 36 (1-2), 80–89.

Gräwe, U., Deleersnijder, E., Shah, S.H.A.M., Heemink, A.W., 2012. Why the Euler scheme in particle tracking is not enough: the shallow-sea pycnocline test case. Ocean Dynamics 62 (4), 501–514.

Gräwe, U., Wolff, J.-O., 2010. Suspended particulate matter dynamics in a particle framework. Environmental Fluid Mechanics 10 (1-2), 21–39.

Holloway, G., 1994. Comment: on modelling vertical trajectories of phytoplankton in a

mixed layer. Deep Sea Research Part I: Oceanographic Research Papers (0967-0637) 41 (5), 957–959. https://doi.org/10.1016/0967-0637(94)90087-6.
Hundsdorfer, W., 2003. Numerical Solution of Time-dependent Advection-Diffusion-Reaction Equations. Springer series in computational mathematics. 1st edition. 33 Springer, Berlin.
Hunter, J., Craig, P., Phillips, H., 1993. On the use of random walk models with spatially variable diffusivity. Journal of Computational Physics 106 (2), 366–376.
Johansen, Ø., Reed, M., Bodsberg, N.R., 2015. Natural dispersion revisited. Marine Pollution Bulletin (0025-326X) 93 (1), 20–26. https://doi.org/10.1016/j.marpolbul.2015.02.026.
Kloeden, P.E., Platen, E., 1992. Numerical Solution of Stochastic Differential Equations. Springer-Verlag Berlin Heidelberg.
Large, W.G., McWilliams, J.C., Doney, S.C., 1994. Oceanic vertical mixing: a review and a model with a nonlocal boundary layer parameterization. Reviews of Geophysics 32 (4), 363–403.
Leifer, I., De Leeuw, G., 2006. Bubbles generated from wind-steepened breaking waves: 1. bubble plume bubbles. Journal of Geophysical Research: Oceans 111 (C6).
Li, Z., Spaulding, M., McCay, D.F., Crowley, D., Payne, J.R., 2017. Development of a unified oil droplet size distribution model with application to surface breaking waves and subsea blowout releases considering dispersant effects. Marine pollution bulletin 114 (1), 247–257.
Lynch, D.R., Greenberg, D.A., Bilgili, A., McGillicuddy Jr, D.J., Manning, J.P., Aretxabaleta, A.L., 2014. Particles in the Coastal Ocean: Theory and Applications. Cambridge University Press.
Mariano, A., Kourafalou, V., Srinivasan, A., Kang, H., Halliwell, G., Ryan, E., Roffer, M., 2011. On the modeling of the 2010 Gulf of Mexico oil spill. Dynamics of Atmospheres and Oceans 52, 322–340.
Maruyama, G., 1955. Continuous Markov processes and stochastic equations. Rendiconti del Circolo Matematico di Palermo 4 (1), 48.
Pavliotis, G.A., 2014. Stochastic Processes and Applications. Springer-Verlag New York.
Pletcher, R.H., 2013. Computational Fluid Mechanics and Heat Transfer, 3rd edition. CRC Press, Boca Raton.
Ramírez, J., Moghimi, S., Restrepo, J.M., Venkataramani, S., 2018. Modelling the mass exchange dynamics of oceanic surface and subsurface oil. Ocean Modelling.
Reed, M., Daling, P.S., Brakstad, O.G., Singsaas, I., Faksness, L.-G., Hetland, B., Ekrol, N., 2000. OSCAR2000: a multi-component 3-dimensional Oil Spill Contingency and Response model. In: Proceedings of the 23rd AMOP Technical seminar, pp. 663–680.
Reed, M., Johansen, Ø., Brandvik, P.J., Daling, P., Lewis, A., Fiocco, R., Mackay, D., Prentki, R., 1999. Oil spill modeling towards the close of the 20th century: overview of the state of the art. Spill Science & Technology Bulletin 5 (1), 3–16.
Restrepo, J.M., Ramírez, J.M., Venkataramani, S., 2015. An oil fate model for shallow-waters. Journal of Marine Science and Engineering 3 (4), 1504–1543.
Röhrs, J., Christensen, K.H., Vikebø, F., Sundby, S., Saetra, Ø., Broström, G., 2014. Wave-induced transport and vertical mixing of pelagic eggs and larvae. Limnology and Oceanography 59 (4), 1213–1227.
Ross, O.N., Sharples, J., 2004. Recipe for 1-D Lagrangian particle tracking models in space-varying diffusivity. Limnology and Oceanography: Methods 2, 289–302.
Scanlon, B., Breivik, Ø., Bidlot, J.-R., Janssen, P.A., Callaghan, A.H., Ward, B., 2016. Modeling whitecap fraction with a wave model. Journal of Physical Oceanography 46 (3), 887–894.
Silverman, B.W., 1986. Density Estimation for Statistics and Data Analysis. Chapman & Hall.
Spaulding, M.L., 1988. A state-of-the-art review of oil spill trajectory and fate modeling. Oil and Chemical Pollution 4 (1), 39–55.
Spaulding, M.L., 2017. State of the art review and future directions in oil spill modeling. Marine pollution bulletin 115 (1-2), 7–19.
Spivakovskaya, D., Heemink, A.W., Deleersnijder, E., 2007. Lagrangian modelling of multi-dimensional advection-diffusion with space-varying diffusivities: theory and idealized test cases. Ocean Dynamics 57 (3), 189–203.
Tennekes, H., Lumley, J.L., 1972. A first course in turbulence. MIT press.
Thomson, D., 1987. Criteria for the selection of stochastic models of particle trajectories in turbulent flows. Journal of Fluid Mechanics 180, 529–556.
Thygesen, U.H., Ådlandsvik, B., 2007. Simulating vertical turbulent dispersal with finite volumes and binned random walks. Marine Ecology Progress Series 347, 145–153.
Tkalich, P., Chan, E.S., 2002. Vertical mixing of oil droplets by breaking waves. Marine Pollution Bulletin 44 (11), 1219–1229.
Tkalich, P., Huda, K., Hoong Gin, K.Y., 2003. A multiphase oil spill model. Journal of Hydraulic Research 41 (2), 115–125.
van Sebille, E., Griffies, S.M., Abernathey, R., Adams, T.P., Berloff, P., Biastoch, A., Blanke, B., Chassignet, E.P., Cheng, Y., Cotter, C.J., Deleersnijder, E., Döös, K., Drake, H.F., Drijfhout, S., Gary, S.F., Heemink, A.W., Kjellsson, J., Koszalka, I.M., Lange, M., Lique, C., MacGilchrist, G.A., Marsh, R., Mayorga Adame, C.G., McAdam, R., Nencioli, F., Paris, C.B., Piggott, M.D., Polton, J.A., Rühs, S., Shah, S.H., Thomas, M.D., Wang, J., Wolfram, P.J., Zanna, L., Zika, J.D., 2018. Lagrangian ocean analysis: fundamentals and practices. Ocean Modelling 121, 49–75.
Versteeg, H., 2007. An Introduction to Computational Fluid Dynamics: The Finite Volume Method, 2nd edition. Pearson/Prentice Hall, Harlow.
Visser, A.W., 1997. Using random walk models to simulate the vertical distribution of particles in a turbulent water column. Marine Ecology Progress Series 158, 275–281.